sciendo

Nordic Concrete Federation

ISSN online 2545-2819
ISSN print 0800-6377

DOI: 10.2478/ncr-2022-0002

Received: March 30, 2022
Revision received: May 31, 2022
Accepted: June 8, 2022

Nonlinear Cyclic Analysis of Reinforced Concrete Columns Using Fiber Section Approach

Ali Vatanshenas
Doctoral Researcher
Faculty of Built Environment, Tampere University
Korkeakoulunkatu 5, 33720, Tampere, Finland
ali.vatanshenas@tuni.fi

ABSTRACT

This study investigates nonlinear modeling and verification of a reinforced concrete element using the fiber section method. At first, the theory related to the fiber section approach and hysteresis models used for cyclic analysis is given. Then, a reinforced concrete column tested previously in the literature is modeled and simulation results are compared with the test results. An acceptable approximation is made utilizing only a few input parameters: Uniaxial stress-strain curves of the materials, location and length of the plastic hinge, and geometry of the model. Moreover, the axial force-moments interaction curve from Eurocode is compared with the one obtained from the nonlinear model. It is shown that by conducting nonlinear analysis a larger capacity of the element is considered which results in a more realistic and economic design.

Key words: Column, Fiber section, Nonlinear analysis, Reinforced concrete, Time history analysis.

1. INTRODUCTION

General modeling techniques are presented in Figure 1 and ordered based on their amount of complexity and computational effort. In the following, only the fiber section approach is investigated.

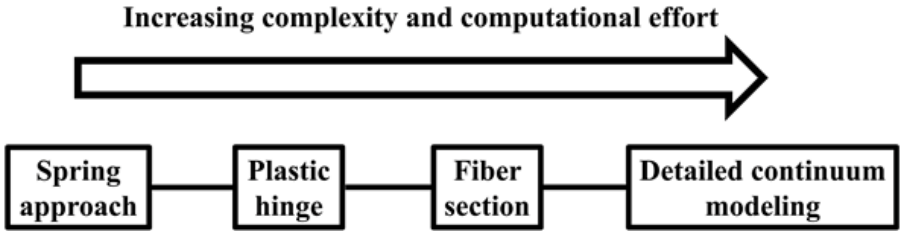

Figure 1 – Modeling approaches order based on complexity and computational effort.

The fiber section approach is based on the finite element method. However, reasonable assumptions are made to obtain satisfactory simulations and reduce the computational effort. In this method, inelasticity is considered at the critical zones of the element, whereas rest of the element is modeled elastically. A cross-section is divided into arbitrary fibers with uniaxial nonlinear behavior defined for each fiber (Figure 2).

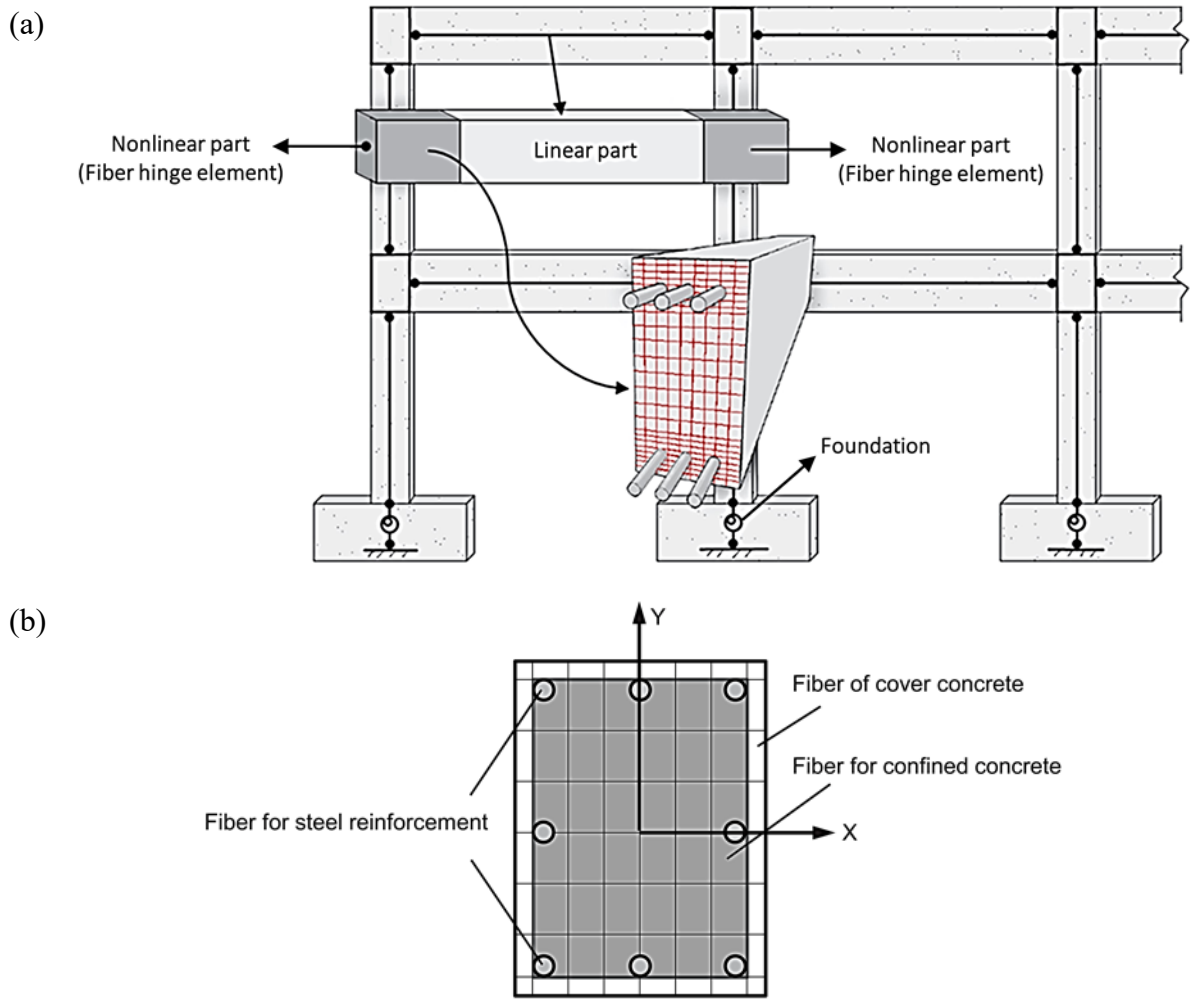

Figure 2 – Schematic of fiber section method: a) modified from [1]*, and b)* [2].

2. THEORY

2.1 Fiber section

Assuming that plane sections remain constant, the following relation for strain ε_i is achieved for each fiber:

$$\varepsilon_i = -\varepsilon_{p+}\phi\, y_i \tag{1}$$

Where ε_p is the strain at the reference point (usually midheight or plastic centroid), ϕ is section curvature, and y_i is the distance between the center of fiber i to the reference point. A schematic of these parameters for a T-shaped beam is shown in Figure 3.

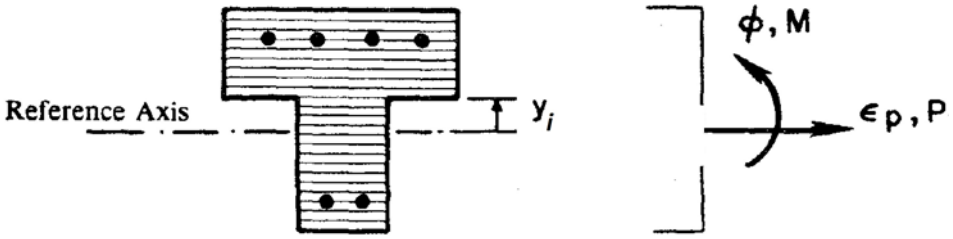

Figure 3 – Presentation of ε_p, ϕ, and y_i for an arbitrary RC section, modified from [3].

Then, incremental axial force dP_s and incremental moment dM_s along the section are obtained by summation of fibers in the section:

$$dP_s = \sum_i A_i E_i\, d\varepsilon_i \tag{2}$$

$$dM_s = \sum_i A_i E_i\, d\varepsilon_i y_i \tag{3}$$

Where A_i and E_i are the area of fiber i and the current modulus of fiber i, respectively. By rewriting the above equations using Eq. 1 we will have:

$$dP_s = \sum_i A_i E_i\, (-d\varepsilon_{p+} d\phi\, y_i) \tag{4}$$

$$dM_s = \sum_i A_i E_i\, y_i (-d\varepsilon_{p+} d\phi\, y_i) \tag{5}$$

By presenting these equations in matrix form we end up with:

$$\begin{Bmatrix} dM_s \\ dP_s \end{Bmatrix} = k_s \begin{Bmatrix} d\phi \\ d\varepsilon_p \end{Bmatrix} = \begin{bmatrix} a_{11} & a_{12} \\ a_{12} & a_{22} \end{bmatrix} \begin{Bmatrix} d\phi \\ d\varepsilon_p \end{Bmatrix} \tag{6}$$

Where the stiffness matrix of the section is simply obtained as:

$$k_s = \begin{bmatrix} a_{11} & a_{12} \\ a_{12} & a_{22} \end{bmatrix} = \begin{bmatrix} \sum_i A_i E_i y_i^2 & \sum_i A_i E_i y_i \\ \sum_i A_i E_i y_i & \sum_i A_i E_i \end{bmatrix} \quad (7)$$

Then, the location (i.e., center) of the plastic hinge along the element and its length l_p are defined by the analyst to relate curvature ϕ to rotation θ and specifying the nonlinear zone of the element (Figure 4).

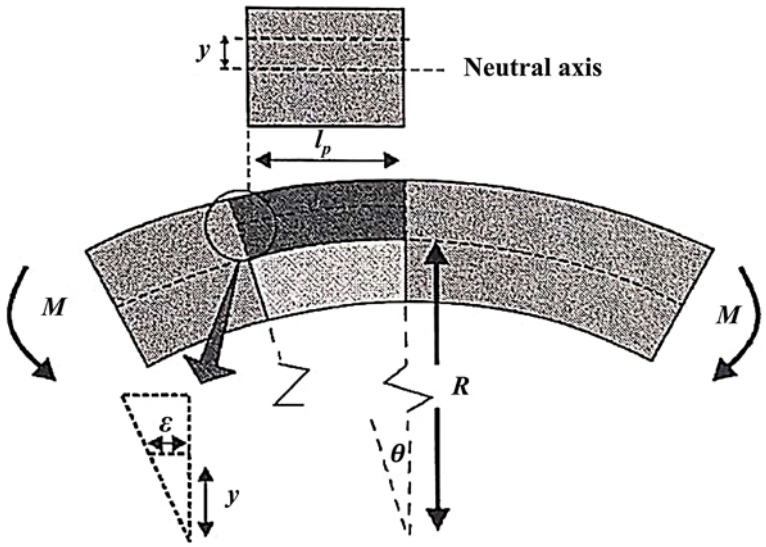

Figure 4 – Schematic of parameters for an element under moment assuming that planes remain constant after applying the load.

$$\phi = \frac{M}{EI} = \frac{1}{R} \quad (8)$$

$$\theta = \frac{l_p}{R} = l_p \phi \quad (9)$$

Where R is curvature radius and EI is flexural rigidity depending on the material and geometry. Plastic hinge length l_p may be obtained from tests or alternatively relations proposed in the literature [1,4]:

$$l_P = \frac{D}{2} \quad (10)$$

$$l_P = 0.05l + \frac{0.1 d_b f_y}{\sqrt{f_c'}} \leq \frac{l}{4} \quad (11)$$

Where D is depth of the section. l is member length, d_b is bar diameter, f_c' is concrete strength, and f_y is steel yield strength.

2.2 Loading-unloading behavior

Takeda model

The Takeda model is formulated for reinforced concrete members and their connections [5]. As shown in Figure 5, the original Takeda model incorporates a trilinear backbone curve. This model approximates cracking of reinforced concrete members, yielding point, and hysteresis behavior via 16 rules. However, these rules do not consider the pinching phenomenon (i.e., stiffness softening after yielding). The unloading-reloading stiffness, K_r is computed via the following relation [6]:

$$K_r = K_{yield}\left(\frac{D_{yield}}{D_{max}}\right)^{0.4} \tag{12}$$

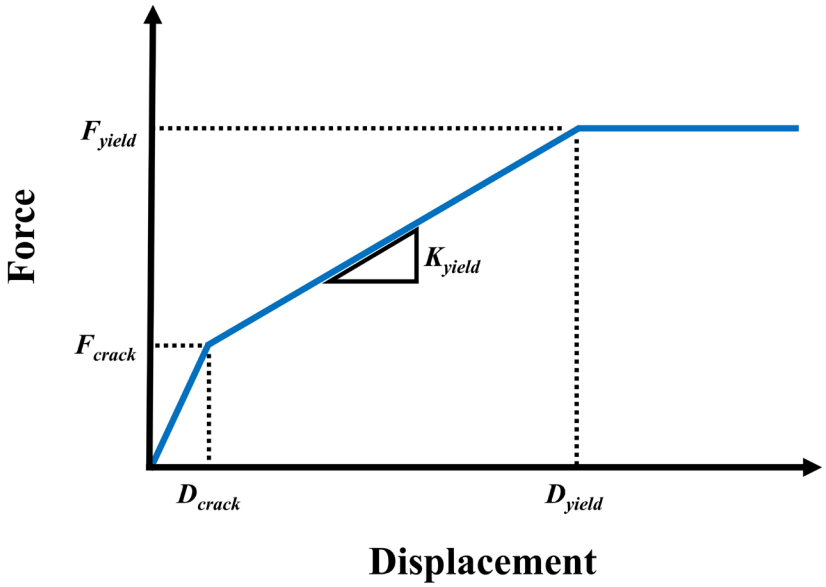

Figure 5 – Takeda model backbone curve.

A modified version of the Takeda model is implemented in the following which assumes constant unloading-reloading part [7]. This modified version is not limited to a trilinear backbone curve and its implementation is quite straightforward.

Pivot model

The Pivot model is formulated for reinforced concrete members as well. This model assumes that linear continuation of all the unloading-reloading lines intersects at one point in space called primary pivot point [8]. This model requires three input parameters to model softening of initial stiffnesses after yielding, defining pivot point, and pinching effects via following parameters: η ($0 < \eta \leq 1$), α ($\alpha \geq 1$), and β ($0 < \beta \leq 1$), respectively. The schematic of Pivot model parameters and their mechanism is illustrated in Figure 6.

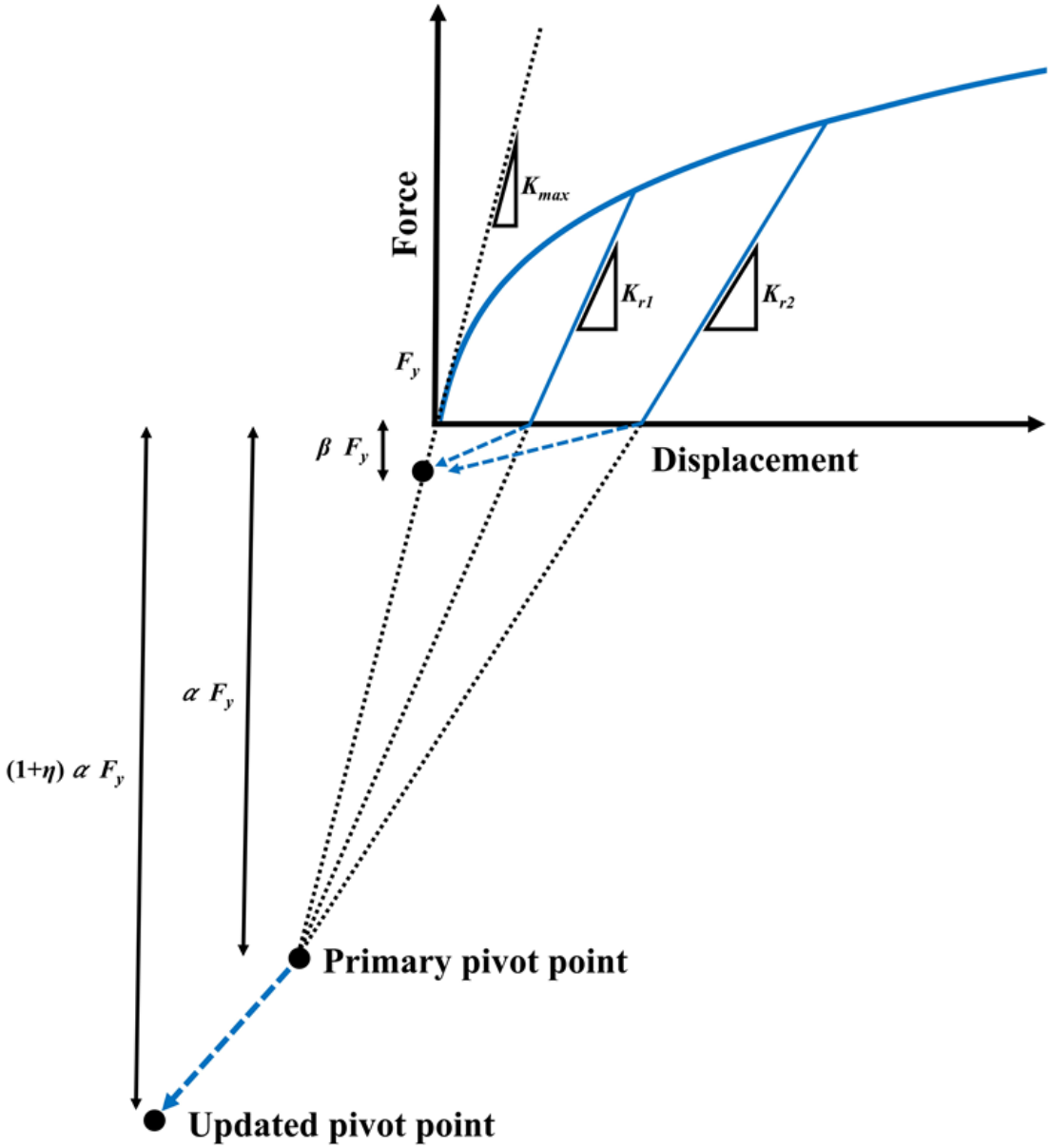

Figure 6 – Schematic of pivot model.

α is a scale factor that defines the height of the pivot point by multiplying into the yield strength, F_y. α is obtained by:

$$\alpha = \left(\frac{K_{r2}\,K_{r1}}{K_{r2} - K_{r1}}\right)\left(\frac{y_1 - y_2}{F_y}\right) \tag{13}$$

Where K_{r1} and K_{r2} are two unloading-reloading stiffnesses. Also, y_1 and y_2 are distances between intersections of unloading-reloading paths with the horizontal axis. Since K_{max} also passes through the pivot point, α can be related to K_{max} by the following equation:

$$\alpha = -\frac{\Omega\,K_{max}\,y_j}{F_y(\Omega - 1)} \tag{14}$$

Where y_j and Ω are the horizontal intersection distance and stiffness degradation ratio corresponding to an arbitrary unloading-reloading stiffness K_{rj}, respectively. Ω is simply computed by:

$$\Omega = \frac{K_{rj}}{K_{max}} \quad ; (0 < \Omega < 1) \tag{15}$$

β controls pinching behavior where $\beta = 1$ neglects pinching phenomenon. According to Figure 6, η updates pivot point to consider softening of initial stiffnesses after yielding. $\eta = 0$ neglects initial stiffness softening effects after yielding.

3. VERIFICATION

In this section, fiber section approach is utilized to simulate a pseudo-static cyclic test on a RC column. The experimental study is performed by [9]. Test schematic before and after the test is presented in Figure 7. As shown in this figure, the damage is concentrated at the bottom of the column. However, a few cracks are also observed on the rest of the element. In addition, the geometry and reinforcement configuration of the column are presented in Figure 8.

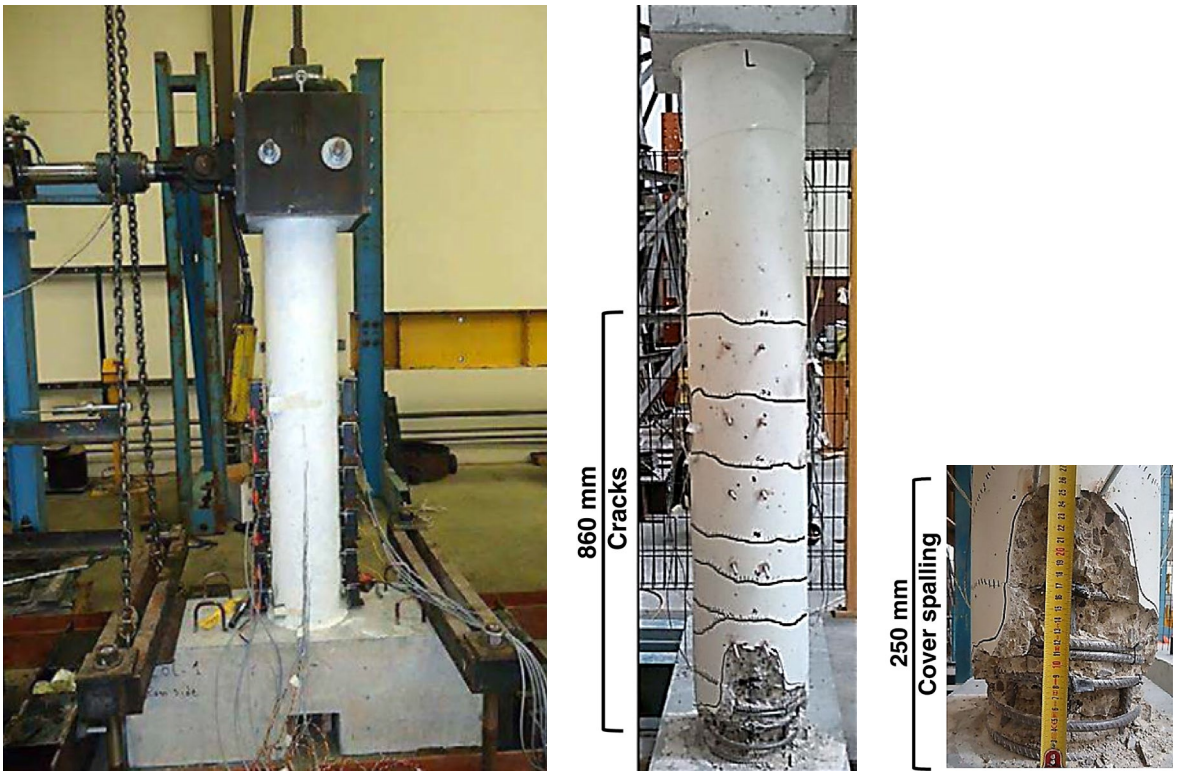

(a) (b)

Figure 7 – RC column specimen: a) before the test, and b) after the test [9].

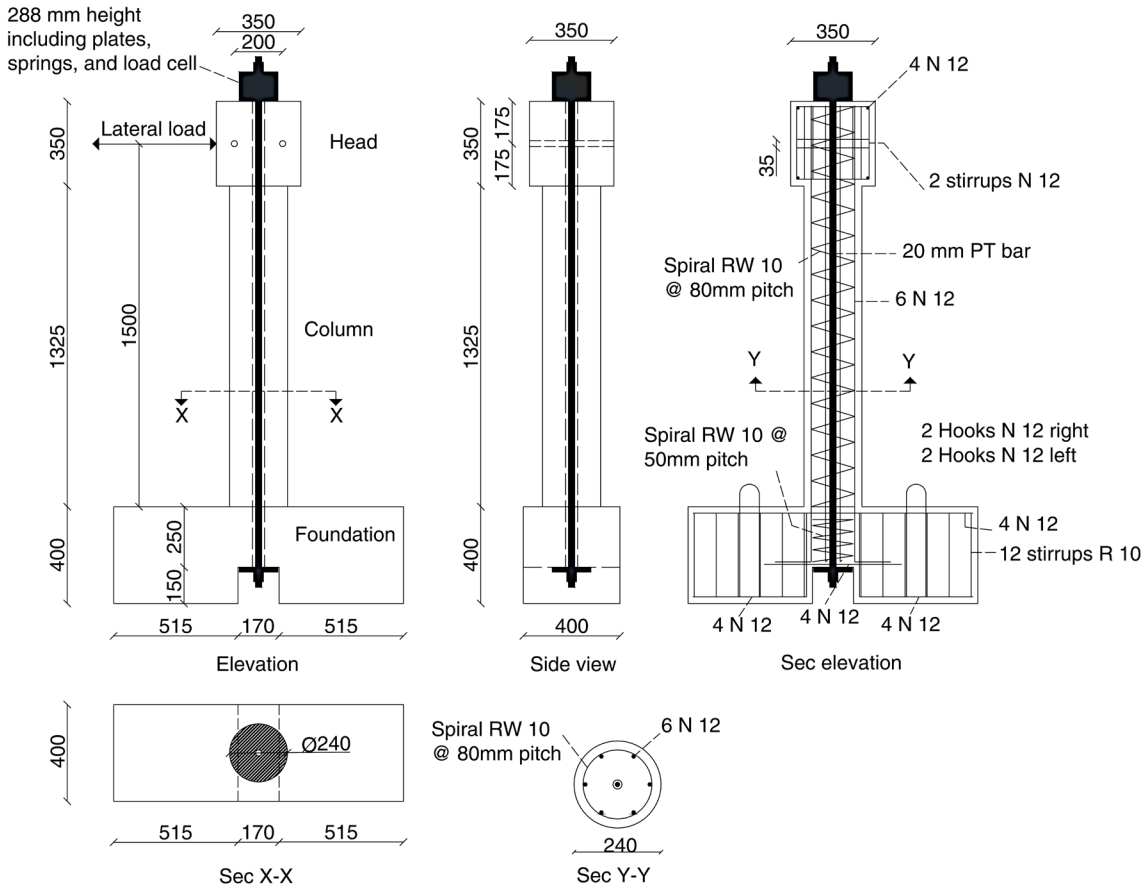

Figure 8 – Column configurations and reinforcement details (units are in mm) [9].

The considered column in this study is labeled as CC-2 in the original study with the material properties given in Table 1. The specimen is first vertically loaded and pseudo-static cyclic loading in horizontal direction is then applied on top of the specimen. Loading history is given in Figure 9a. In addition, the input energy plot obtained from the numerical analysis is shown in Figure 9b. Both plots indicate an increasing trend as the loading steps proceed.

Table 1 – Material properties reported in the experimental study [9].

Material name	f_c' **(*MPa*)**	***E* (*GPa*)**	f_y **(*MPa*)**	ε_y **(-)**	f_u **(*MPa*)**	ε_u **(-)**
Concrete	61.9	45.62	-	-	-	-
Longitudinal rebar	-	200	550	0.00275	698	0.11600
Spiral rebar	-	200	612	0.00306	641	0.02680

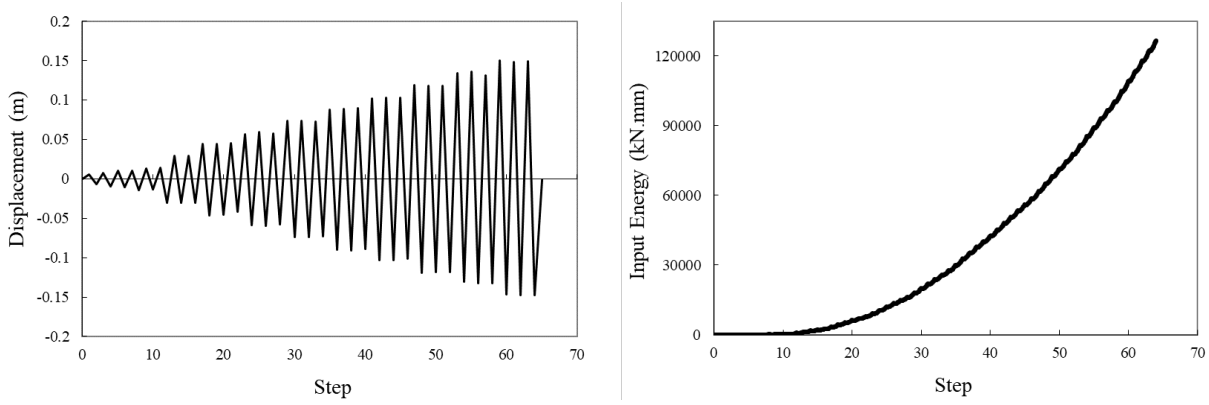

Figure 9 – Pseudo-static cyclic loading: a) displacement plot, and b) input energy plot.

The schematic of the model is illustrated in Figure 10. Two concrete materials are defined based on the Mander's model [10] for confined and unconfined concretes. Rebar material is also defined according to the Park's model which its formulation is available in [11]. In addition, the length of the fiber plastic length is assumed to be 0.24 *m* according to the test result presented in Figure 7b and its location is considered as 0.15 of the column's height. As mentioned earlier, a few cracks are also observed out of the plastic zone. Therefore, a cracking factor equal to 0.7 is used to reduce the moment of inertia in the elastic portion of the element.

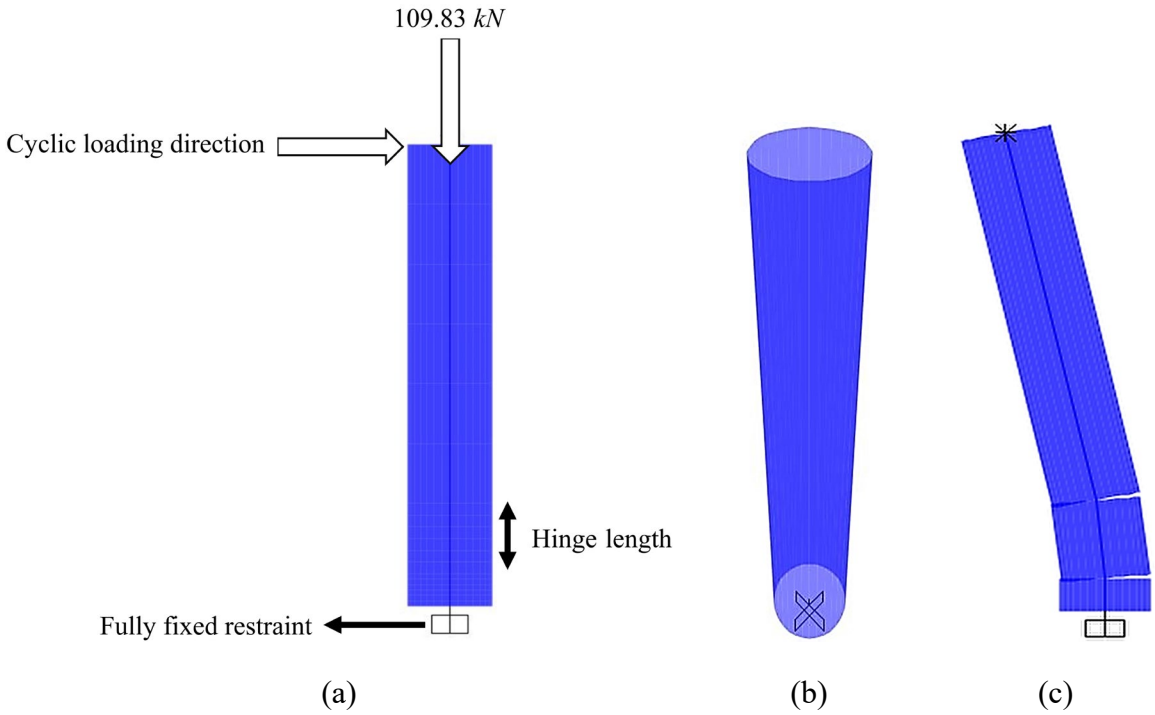

Figure 10 – RC column model: a) 2D presentation including loading and fiber plastic hinge zone, b) 3D presentation, and c) deformed configuration after analysis.

Takeda and Pivot (assuming α=15, β=1, and η=0.7) hysteresis models are used for concrete and rebars, respectively [5,8]. Comparison between hysteresis curves obtained from the simulation and experiment are illustrated in Figure 11. A slightly stiffer response at the beginning of the estimation plot is observed which might be due to neglecting bond-slip of rebars. Nevertheless, an acceptable approximation is achieved from the simulation.

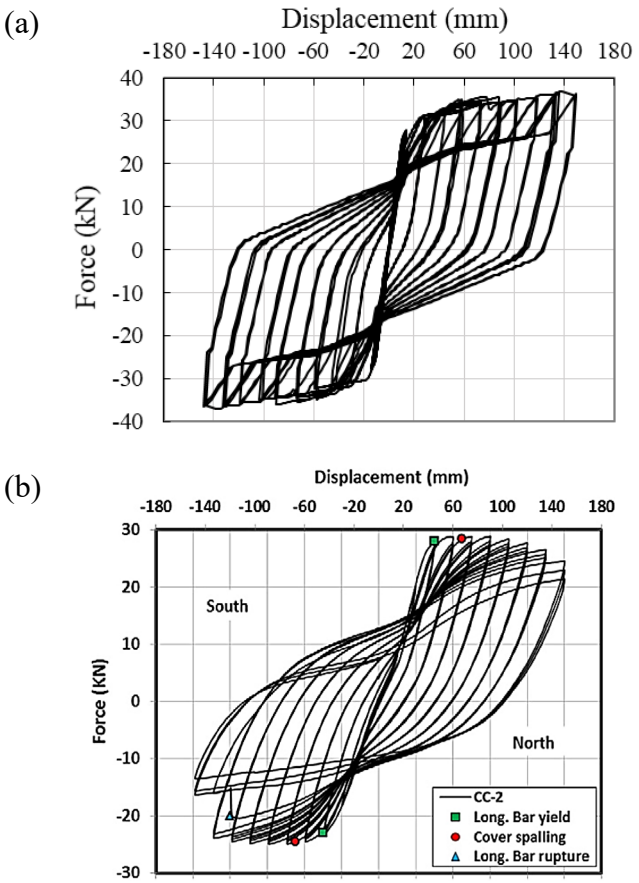

Figure 11 – Comparison of hysteresis behaviors: a) estimation, and b) test result, modified from [9].

4. RESULTS AND DISCUSSION

4.1 Hinge results

The fiber section approach uses the materials stress-strain curve directly as an input. As a result, the moment-curvature (M-ϕ) relationship is not predefined, and simulation can be conducted with the constant or varying axial load automatically. Hinge behavior under axial load and moment is given in Figure 12. As shown in this figure, the fiber section approach considers nonlinear coupling of axial force and moment successfully.

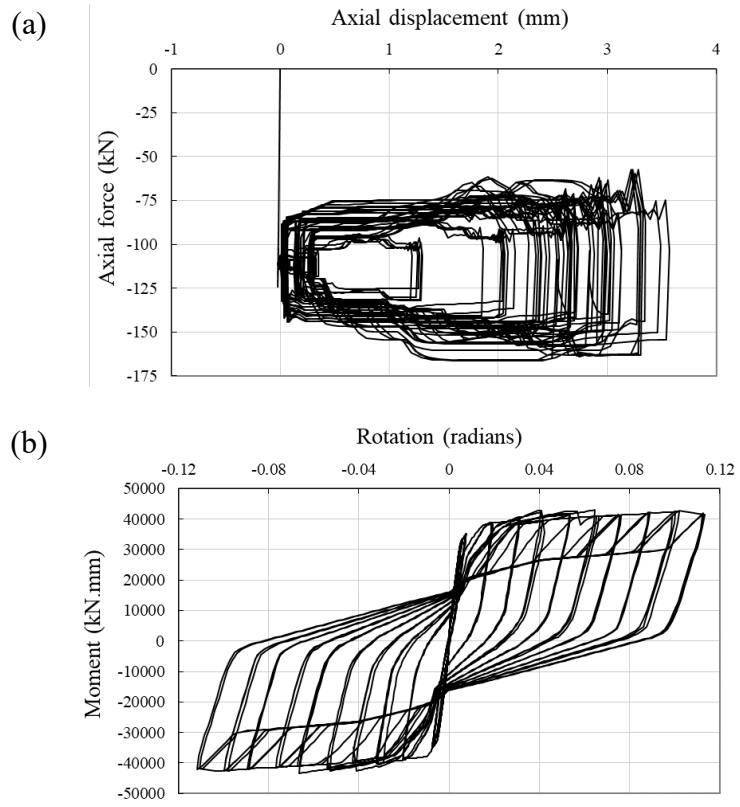

Figure 12 – Fiber section simulation: a) axial force-displacement, and b) moment-rotation.

In total, thirty six fibers are used for idealizing the section: Eight fibers for rebars, 16 fibers for confined concrete, and twelve fibers for unconfined concrete regions. Analysis results for each individual fiber are available. For instance, the cyclic stress-strain response of three fibers related to rebar, confined concrete, and unconfined concrete indicated in Figure 13 are given in Figure 14. As shown in these plots, defined behaviors for fibers are converged adequately. However, negligible overshooting is observed for rebar in the transition domain from the elastic threshold to the hardening zone. Moreover, failure in unconfined concrete is not simulated as sharp unloading as defined curve and a smooth unloading path is followed at the end. Nevertheless, the approximation is satisfactory.

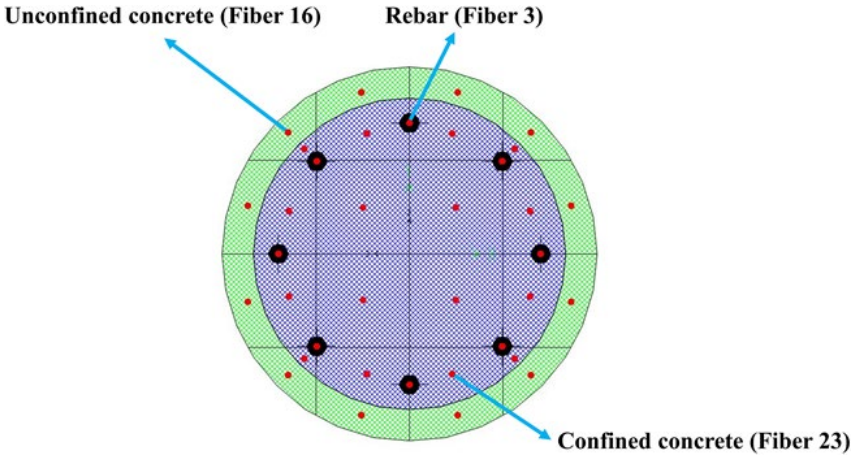

Figure 13 – Configuration of fibers distributed along the section.

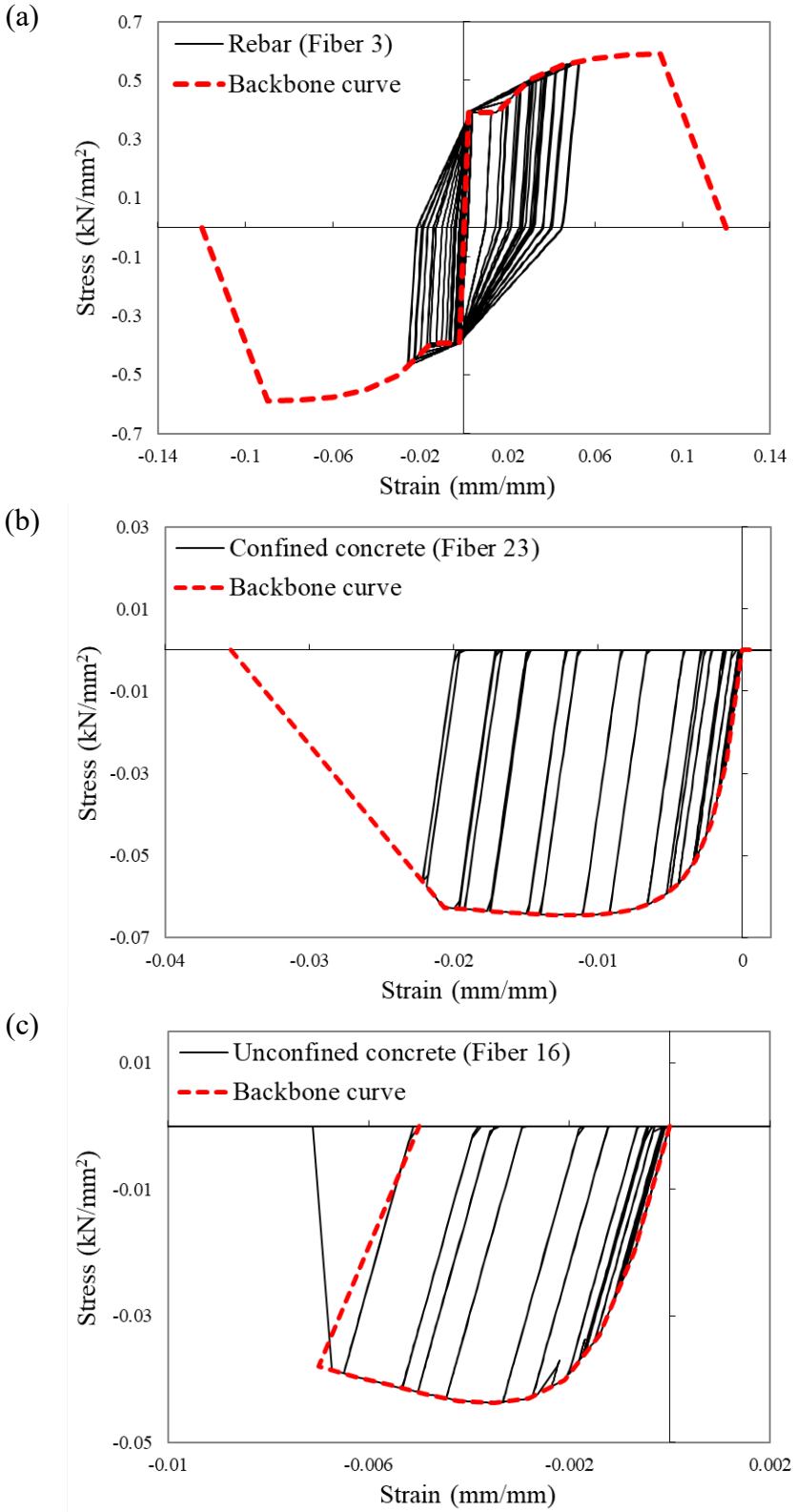

Figure 14 – Fibers' hysteresis response: a) rebar, b) confined concrete, and c) unconfined concrete. In addition, the backbone curve introduced before the analysis is plotted to evaluate the convergence of the results.

4.2 Axial force-moments (P-M_2-M_3) interaction

In general, failure mode in structures is dominated by geometry, materials, and lateral resisting systems. For instance, in short columns, shear forces govern the failure mode or in concentrically braced systems axial forces generated in the columns and braces cause failure under lateral loading [12,13]. Nevertheless, for ordinary columns in routine design (i.e., moment frame systems) failure occurs due to the interaction of axial force and moments in horizontal directions (P-M_2-M_3). By plotting different combinations of failure axial forces and moments, a surface is obtained in 3D space known as capacity surface. With respect to this surface three conditions might occur:

1- Interaction point situated inside the capacity surface ➔ Capacity > Demand

2- Interaction point situated on the capacity surface ➔ Capacity = Demand

3- Interaction point situated outside the capacity surface ➔ Capacity < Demand

For symmetric cross sections, the 3D interaction surface can be replaced by a 2D plot for simpler interpretation. Figure 15 illustrates the important points in the interaction curve in 2D:

- Pure tension: Only axial force in tension occurs at this point.
- Pure compression: Only axial force in compression occurs at this point.
- Pure bending: Axial force is zero at this point and the section needs to tolerate bending moments only.
- Balanced failure: At this point rebars yield in tension and concrete in compression reaches its ultimate strain.

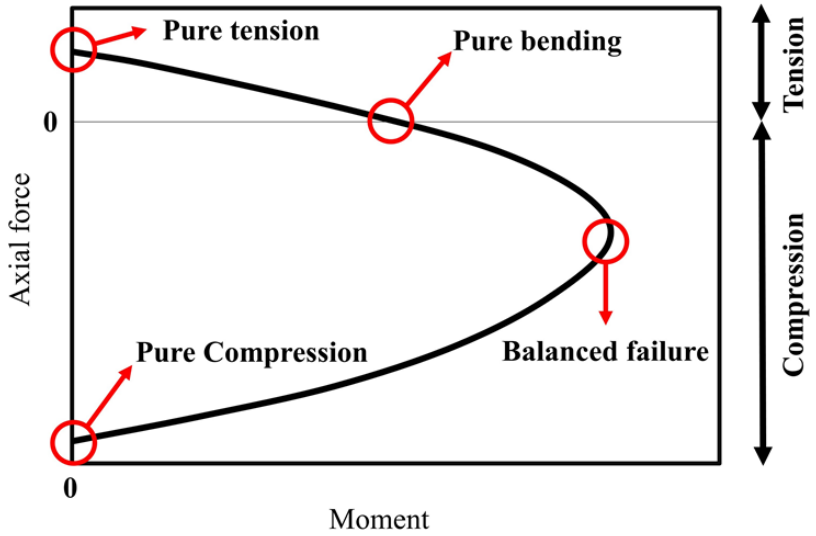

Figure 15 – Capacity curve in 2D including important points.

This type of interpretation is widely used for designing structures. Different design codes introduce different safety factors to reduce the capacity of the structural elements which ends up with conservative and unrealistic designs. For instance, by considering the concrete frame design for Eurocode 2-2004 [14], and specific national Annex specified for Finland region, interaction

surface is reached. Figure 16 illustrates the axial force-moment interaction curves obtained from Eurocode and fiber section approach for the considered column for verification. As shown in this figure, Eurocode underestimates the capacity curve significantly. On the other hand, the fiber section approach considers a more realistic estimation of capacity since materials nonlinearity is exploited directly in the model. Since the considered section is symmetric the 2D plot of axial force-moment is also given for easier interpretation. As shown in Figure 16c, Eurocode scales down the compression capacity significantly. For instance, for the case of pure axial compression force, Eurocode considers 39% less capacity compared to the fiber section approach. This means by conducting nonlinear analysis not only more realistic results are obtained but the more economical design is expected as well.

(a)

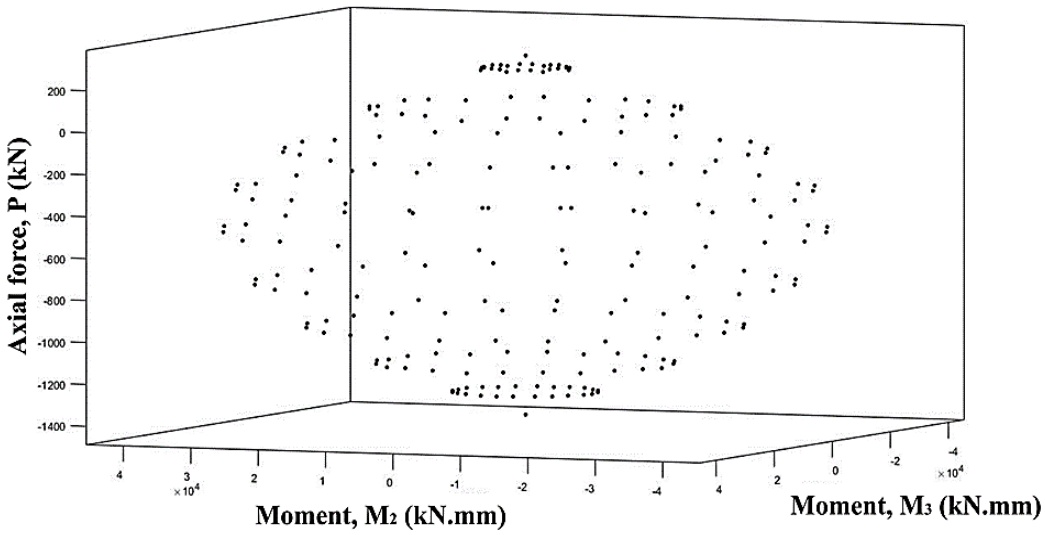

(b)

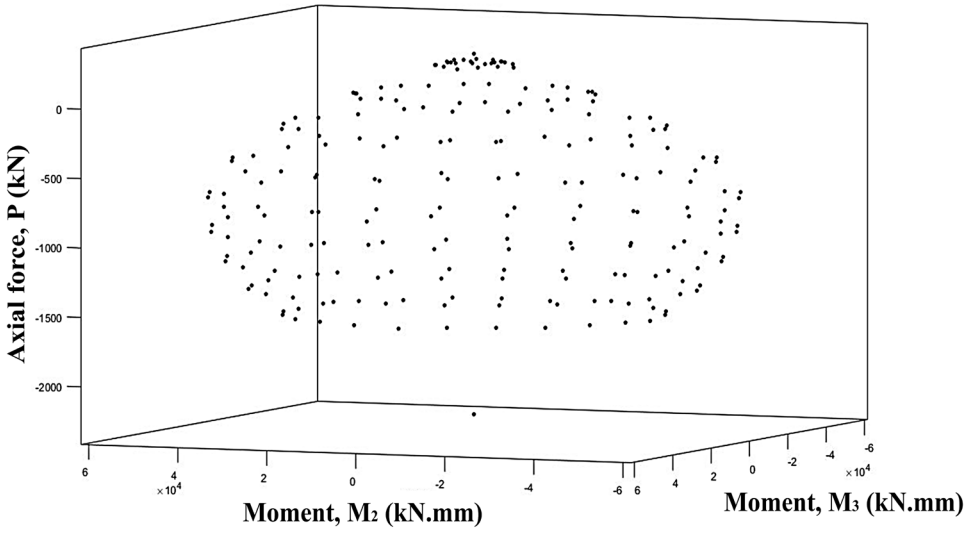

(c)

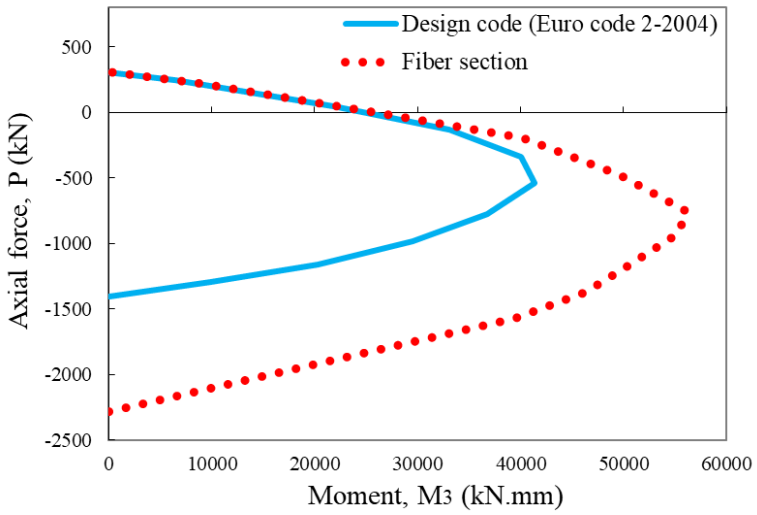

Figure 16 – Axial force-moment interaction curves: a) P-M_2-M_3 surface based on Eurocode, b) P-M_2-M_3 surface based on fiber section approach, and c) Capacity curves in 2D.

5. CONCLUSIONS

Nonlinear modeling of an RC section was investigated in this study. Few and easily obtainable parameters (uniaxial stress-strain curve, location and length of plastic hinge, and geometry of the section) are required for the fiber section approach. Satisfactory results are obtained by only a few fibers. The fiber section approach could simulate axial force-moment interactions for RC columns under cyclic loading using two hysteresis models: Takeda and Pivot. Also, progressive failure within the section is monitored from cracking of the cover until yielding of rebars. Nevertheless, the fiber section method has also some limitations. For instance, it is assumed that plane sections remain plane during the analysis, shear and torsional behaviors are assumed linear. In addition, modeling rebars' bond-slip and buckling in RC members are not straightforward. However, such behaviors may be modelled by calibrating the material nonlinear stress-strain curve or adding springs to the model.

ACKNOWLEDGEMENT

The author acknowledges financial support from Tampere University.

REFERENCES

1. Guidelines for nonlinear structural analysis and design of buildings: "part IIb - reinforced concrete moment frames (PY - 2017 PB)". National Institute of Standards and Technology (NIST), 2017.
2. Lin X & Lu X: "Numerical Models to Predict the Collapse Behavior of RC Columns and Frames". *The Open Civil Engineering Journal*. No. 11(1), 2017.
3. Kaba S A & Mahin S A: "Refined modelling of reinforced concrete columns for seismic analysis". University of California, Earthquake Engineering Research Center. 1984.
4. Berry M P & Eberhard M O: "Performance Modeling Strategies for Modern Reinforced Concrete Bridge". University of California, Berkeley. 2008.
5. Takeda T, Sozen M A & Nielsen N N: "Reinforced concrete response to simulated earthquakes". *Journal of the Structural Division*. No. 96(12), 1970, pp. 2557-2573.
6. Sengupta P & Li B: "Hysteresis Modeling of Reinforced Concrete Structures: State of the Art". *ACI Structural Journal*. No. 114(1). 2017.
7. Hopper M W: "Analytical models for the nonlinear seismic response of reinforced concrete frames". Pennsylvania State University. 2009.
8. Dowell O K, Seible F & Wilson E L: "Pivot hysteresis model for reinforced concrete members". *ACI Structural Journal*. No. 95, 1998, pp. 607-617.
9. Youssf O, ElGawady M A & Mills J E: "Experimental investigation of crumb rubber concrete columns under seismic loading". *InStructures*., No. 3, 2015, pp. 13-27.
10. Mander J B, Priestley M J & Park R: "Theoretical stress-strain model for confined concrete". *Journal of Structural Engineering*. No. 114(8), 1988, pp. 1804-1826.

11. Computers and Structures, Inc. (CSI): “Technical Note Material Stress-strain Curves”. Berkeley, California, USA. 2008.
12. Vatanshenas A, Mori T & Murota N: “Structural rehabilitation using high damping rubber bearing (HDRB)”. *Bulletin of the New Zealand Society for Earthquake Engineering*. No. 54(1), 2021, pp. 49-57.
13. Vatanshenas A, Heydarian H & Tafreshi S T: “Seismic rehabilitation by steel jacketing method affected by different base support conditions using pushover analysis”. *American Journal of Engineering Research (AJER)*. No. 7 (5), 2018, pp. 208-212.
14. Eurocode 2: “Design of concrete structures (EN 1992)”. European Committee for Standardization. 2004.